Multisectional Modeling of High-Speed Electrooptic Modulators Integrated in a Microwave Circuit CAD Environment

Marco Pirola, *Member, IEEE*, Federica Cappelluti, *Member, IEEE*, Giovanni Giarola, and Giovanni Ghione, *Senior Member, IEEE*

***Abstract*—We present a new multisectional model for high-speed electrooptic modulators, fully integrated within the framework of a microwave circuit computer-aided design (CAD) suite (MWOFFICE [1]). Starting from geometrical and layout parameters, the model allows both simple (traveling-wave) and complex (phase reversal, periodically loaded) structures to be assembled, analyzed, and optimized from the standpoint of the electrical and electrooptic response (including chirp effects) both in small-signal (analog) and in large-signal (digital) operation, exploiting standard simulator tools. At no additional effort, parasitic and passive elements (such as optical or electrical delay paths) can be directly included in the modulator schematic, and the effect of transitions and package parasitics can be readily accounted for at a circuit level. Moreover, model integration within a circuit CAD suite enables one to seamlessly perform driver and modulator design and optimization within the same monolithic or hybrid circuit environment. Comparisons with experimental and literature data and design examples are presented to validate the approach and stress its potential in the design of high-speed electrooptic modulators.**

***Index Terms*—Amplitude modulation, design automation, electrooptic effects, electrooptic modulation, harmonic analysis, microwave modulation, optical communication, phase modulation, simulation software.**

I. Introduction

THE radio-frequency (RF) modulation of optical signals through external modulators plays a fundamental role in both digital and analog high-speed fiber-optic transmission systems. At present, among the several technological solutions proposed, electrooptic modulators, above all those exploiting ferroelectric materials such as lithium niobate, still exhibit overall superior system properties in terms of extinction ratio and chirp. This paper will therefore focus on the modeling of electrooptic amplitude modulators, with particular attention to lithium niobate ($LiNbO_3$)-based devices.

High-speed electrooptic Mach–Zehnder modulators are distributed structures, wherein the RF signal travels along a transmission line interacting with the optical signal conveyed by an optical waveguide. The microwave field modifies the optical refractive index through the electrooptic effect, and two phase modulated optical beams are combined, thus achieving amplitude modulation through interference. Unless the structure is completely symmetrical, a residual, time-dependent phase modulation affects the output signal, causing frequency chirp. A Mach–Zehnder amplitude modulator is sketched in Fig. 1; the output RF port is usually closed on a matched load.

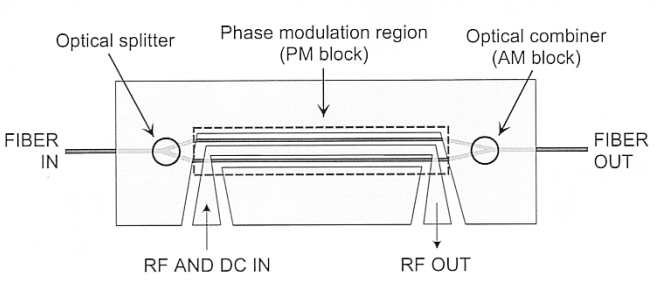

Fig. 1. Electrooptic Mach–Zehnder amplitude modulator structure.

The microwave design of the active interaction region affects the modulator performances both in terms of modulation bandwidth and of driving voltage (on–off voltage or V_π). Moreover, optimization of the modulator cross-section alone, which can be obtained through electromagnetic analysis tools based on quasi-static or full-wave approaches (see, e.g., [2] and references therein), does not completely solve the design problem, since parasitic effects arise due to transitions, bends, tapers, real loads, and other package-related features. Even more complex is the design of *phase-reversal* [3], *periodically loaded* [4], or *resonant* [5] modulator structures, whose layout includes modulating line sections, delay blocks (e.g. transmission line stubs), and often matching elements. Although approximate design strategies and stand-alone models have been proposed for simple traveling-wave structures [6], [7] and resonant modulators [5], there is a complete lack, as far as the authors' knowledge goes, of a global, multisectional computer-aided design (CAD) model fully integrated within a microwave circuit design environment and able to carry out the analysis (small-signal or large-signal) and geometrical optimization of arbitrarily complex modulator structures. Besides its interest in modulator design, an integrated CAD model also allows for the codesign of the driver amplifier and of the modulator, an important issue in high-speed low-impedance structures, where the insertion loss related to 50-Ω package connections would suggest integration between the driver and modulator stages.

Manuscript received April 17, 2003; revised July 28, 2003. This work was supported in part by the Center of Excellence on Multimedia Radio Communications, Politecnico di Torino, under Project Line WP-2.

The authors are with the Dipartimento di Elettronica and CERCOM, Politecnico di Torino, 10129 Torino, Italy.

Digital Object Identifier 10.1109/JLT.2003.820044

In this paper, we propose a new CAD modulator model able to predict the device response starting from the layout and line geometry. The model has been implemented as a user-defined component within the framework of the MWOFFICE *design suite* [1], but the modeling strategy can be easily extended to any microwave and RF circuit CAD simulator implementing user-defined models.

The model formulation, discussed in Section II, allows for frequency-domain small-signal and large-signal (HB) analysis, including eye-diagram evaluation in the presence of digital input signal and distortion estimate for analog applications; moreover, tuning, optimization, coupling with internal or external EM models, yield, and sensitivity analysis with respect to geometrical parameters, can be readily carried out with standard tools. The modulator response includes not only optical power modulation, but also chirp. After a few details concerning the CAD implementation (Section III), the model is validated in Section IV through a comparison between the small-signal modeled and measured performance of a high-speed $LiNbO_3$ Mach–Zehnder modulator. An analysis of the modulator linearity under two-tone RF excitation is also presented. Moreover, large-signal simulations, showing the capability of the approach to accurately predict frequency chirping, are presented through a comparison with literature data. Finally, the design of a periodically loaded modulator taken from the literature is replicated within the CAD environment.

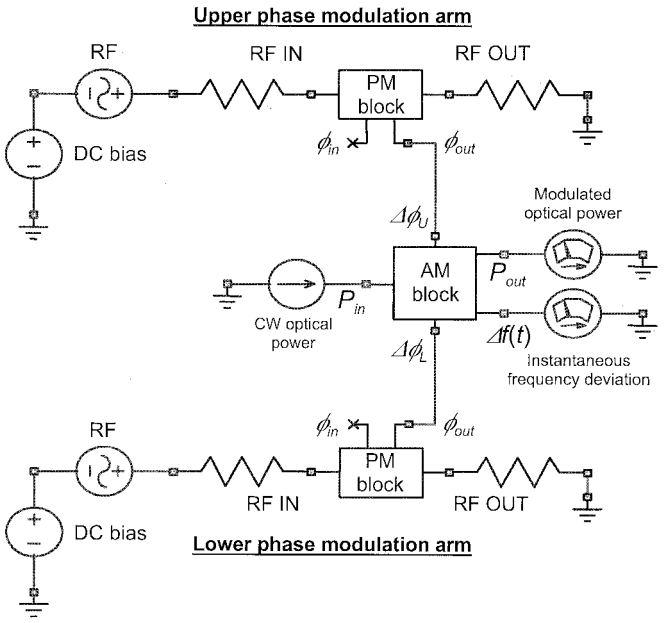

Fig. 2. Schematic of a Mach–Zehnder amplitude modulator with two uniform phase modulating paths, showing the phase-modulation (PM) and interference (AM) blocks. Notice that the optical input of the PM blocks (see Fig. 3) is zero (i.e., is left open), since this corresponds to initial zero phase modulation along the PM region.

II. The Model

The theory of electrooptical interaction in a distributed structure is well established. Analytical expressions for the small-signal frequency response of an uniform modulator section with given load and generator impedances are easily derived as a combination of two *sinc* functions of frequency, and are widely exploited for modulator ad hoc optimization. In this regard, it is worth remembering that the frequency-dependent small-signal amplitude modulation index $m(f)$ corresponds to the phase modulation frequency response [8]. On the other hand, in large-signal operation, the amplitude modulation response is nonlinear (besides being frequency-dispersive), since optical interference results in a raised cosine law relating the normalized input modulator voltage V/V_π and the output optical intensity. On the whole, the development of a CAD small- and large-signal multisectional model of interferometric modulators must deal with the following issues. First, the *nonlinear* and *dispersive* nature of the modulator response cannot generally be handled in a direct manner by most RF circuit or system simulators, wherein only memoryless (nondispersive) nonlinear blocks *or* dispersive linear blocks are allowed for. Therefore, the model must be suitably partitioned, also in accordance with the physical structure of the modulator, in which the phase delay and interference blocks are separate. Then, the model for the interaction region section must be local, i.e., it must depend on the input and output total section voltages rather than on generator and load conditions, which have to be imposed at a network level. In other words, the model must be compatible with a circuit simulator based, e.g., on nodal analysis. This is in contrast with the "resonant cavity" modeling approach in [6], which requires the generator and load impedances as seen from each section to be evaluated explicitly. Finally, a suitable electrical model has to be implemented for the optical line, since this component does not exist as such in microwave CAD environments; to that purpose, electrical variables must be associated to optical signals, such as the optical phase modulation, the optical power, and the frequency chirping. In what follows, electrical variables (ports) exploited to describe optical variables (ports) will be referred to, for the sake of semplicity, as optical variables (ports).

In the present approach, the above issues have been addressed as follows. Within the conventional complex envelope representation (see, e.g., [9]), the optical signal power and slowly varying phase are expressed (in the frequency domain) as RF currents having the same frequency as the input RF signal. The modulator is modeled as the interconnection of two devices.

1) The *phase-modulation block* (PM block; see Fig. 2) is a four-port (two electrical, two optical) driven by the port electrical voltages, which provides, at the output optical port, the total PM $\phi_{\rm out}$ (expressed as a current) resulting from adding the PM of the active section $\Delta\phi$ to the input PM $\phi_{\rm in}$ (expressed as a current). The output PM also includes the group delay related to the optical signal propagation along the active region. The PM block can be cascaded and/or intermixed with other circuit elements (delay lines, stubs, transitions, etc.).
2) The *interference block* (AM block; see Fig. 2) is a five-port, having as inputs two optical signals (RF currents) $\Delta\phi_U, \Delta\phi_L$ representing the total phase modulation along two different paths (corresponding, e.g., to the upper and

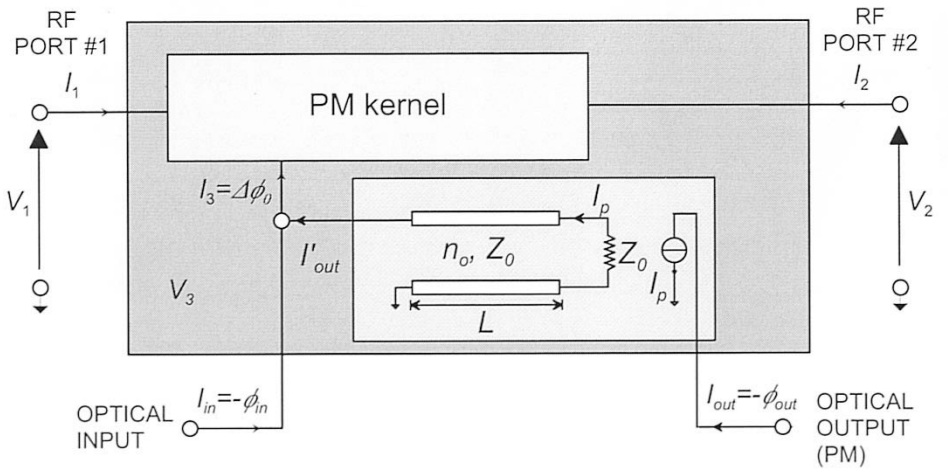

Fig. 3. Phase modulation block; the optical inputs and phase-modulated outputs are associated to proper RF currents so as to allow the block to work as a single frequency linear device.

lower arm of a Mach–Zehnder modulator), and a dc current signal $P_{\rm in}$ representing the continuous-wave input optical power; the two output ports yield time-varying optical (current) signals $P_{\rm out}$ and $\Delta f(t)$ describing, respectively, the AM optical output power resulting from interference, and the instantaneous frequency deviation.

As a first example, the two blocks (PM and AM) can be exploited to model a simple dual-drive amplitude modulator with two different phase modulation paths according to the schematic shown in Fig. 2. Globally, therefore, the amplitude modulator is modeled as a cascade of modulating and/or nonmodulating PM sections along two paths, and an AM device performing beam interference. Optical nonmodulating delay sections can be easily introduced along the path of the optical signal under the form of ideal, matched transmission lines (see next section).

A. Phase-Modulation Block

The equivalent circuit of the PM block is shown in Fig. 3. It can be partitioned into two parts: the *PM kernel*, which provides the (undelayed) electrooptic phase modulation $\Delta\phi_0 = I_3$ as a function of the input and output voltages V_1 and V_2; and an optical delay line, accounting for the propagation delay of the optical signal envelope along the interaction region. For the sake of simplicity, the optical line is supposed to be matched.

From the electrical standpoint, the PM block simply is a transmission line of length L. Concerning the electrooptic interaction, the phase modulation of the optical signal due to the electrically induced refractive index change along the optical waveguide can be expressed as (see, e.g., [8])

$$\Delta\phi(t_0) = -\frac{\pi}{\lambda_o}\frac{n_o^3 r\Gamma}{G}\int_0^L v_m(z,t_0)\mathrm{d}z \qquad (1)$$

where $v_m(z,t_0) \equiv v_m(z, t = t_0 + z/v_o)$ is the *delayed* microwave voltage, as seen by the optical signal envelope traveling at group velocity v_o and entering the modulator at $t = t_0$; r is the electrooptical Pockels coefficient; G is the coplanar line gap; Γ is the overlap integral between the microwave and optical fields; and λ_o and n_o are, respectively, the wavelength and the modal group optical refractive index.

Through straightforward transmission line theory, the total (delayed) RF voltage on the interaction line $v_m(z,t_0)$ and thus the associated phasor $V_m(z)$ can be readily expressed as a linear combination of the total input and output voltages V_1 and V_2, respectively. By inserting such an expression into (1), the phasor $\Delta\phi$ corresponding to the total phase modulation $\Delta\phi(t_0)$ at the output of an interaction section of length L can be shown to linearly depend on the total voltages at the input and output of the section as

$$\Delta\phi = \Delta\phi_0 \mathrm{e}^{-\mathrm{j}\omega\frac{n_o}{c}L} = \left[V_1\xi_1(f) + V_2\xi_2(f)\right]\mathrm{e}^{-\mathrm{j}\omega\frac{n_o}{c}L} \qquad (2)$$

where c is the free-space light velocity and ξ_1 and ξ_2 depend on the modulation frequency as

$$\xi_1(f) = \frac{\pi}{\widetilde{V}_\pi}\frac{\Psi(\nu_-)\mathrm{e}^{\gamma_m L} - \Psi(\nu_+)\mathrm{e}^{-\gamma_m L}}{\mathrm{e}^{\gamma_m L} - \mathrm{e}^{-\gamma_m L}}$$
$$\xi_2(f) = \frac{\pi}{\widetilde{V}_\pi}\frac{-\Psi(\nu_-) + \Psi(\nu_+)}{\mathrm{e}^{\gamma_m L} - \mathrm{e}^{-\gamma_m L}}$$

where $\Psi(\cdot)$ and $\nu_\pm$ are defined as

$$\Psi(\nu_\pm) = \frac{1}{\nu_\pm}\left(1 - \mathrm{e}^{\nu_\pm}\right)$$
$$\nu_\pm(f) = (\pm\gamma_m + \mathrm{j}\beta_o)L.$$

In the previous expressions, $\widetilde{V}_\pi$ is the driving voltage corresponding to a π phase shift on the interaction section,[1] $\gamma_m = j\beta_m - \alpha_m$ is the complex microwave propagation constant, and $\beta_o = \omega/v_o$.

[1]Notice that in a symmetric Mach–Zehnder modulator the on–off voltage is $V_\pi = \widetilde{V}_\pi/2$.

In order to implement (2) in a circuit environment, we define the PM kernel as a linear three-port (two electrical, one optical) having the following admittance parameters:

$$\begin{bmatrix} I_1 \\ I_2 \\ I_3 \end{bmatrix} = \begin{bmatrix} Y_{11} & Y_{12} & 0 \\ Y_{21} & Y_{22} & 0 \\ \xi_1 & \xi_2 & 0 \end{bmatrix} \begin{bmatrix} V_1 \\ V_2 \\ V_3 \end{bmatrix}. \tag{3}$$

The admittance matrix can be partitioned into two submatrices:

1) the admittance matrix of a lossy transmission line section of length L

$$\begin{bmatrix} Y_{11} & Y_{12} \\ Y_{21} & Y_{22} \end{bmatrix} = \frac{Y_0}{1-\mathrm{e}^{-2\gamma_m L}} \begin{bmatrix} 1+\mathrm{e}^{-2\gamma_m L} & -2\mathrm{e}^{-2\gamma_m L} \\ -2\mathrm{e}^{-2\gamma_m L} & 1+\mathrm{e}^{-2\gamma_m L} \end{bmatrix}$$

where Y_0 is the line characteristic admittance;

2) a submatrix yielding the undelayed, i.e., referred to the input of the interaction section, phase modulation $\Delta\phi_0 \equiv I_3$ according to (2)

$$I_3 = [\xi_1\ \xi_2] \begin{bmatrix} V_1 \\ V_2 \end{bmatrix}.$$

Notice that the conventional analytical expression for the phase-modulation response of a homogeneous modulator of length L terminated by an input generator and an output load can be readily obtained from (3) by relating the input (output) voltages and current through the generator (load) conditions, respectively.

In addition to the PM kernel, the PM block includes an optical delay line characterized by the transfer function

$$I_{\mathrm{out}} = I'_{\mathrm{out}} \mathrm{e}^{-\mathrm{j}\omega \frac{n_o}{c} L}$$

(see Fig. 3) whose equivalent circuit consists of an ideal, lossless transmission line terminated on a matched load to avoid reflections; it also contains a current-controlled current source (CCCS) buffer to provide complete decoupling from subsequent stages, i.e., to make the optical line unidirectional. The line phase velocity corresponds to the optical group velocity.

In conclusion, the input and output phase modulations of the optical signal traveling through the interaction section ($\phi_{\mathrm{in}} = -I_{\mathrm{in}}, \phi_{\mathrm{out}} = -I_{\mathrm{out}}$) are related as (see Fig. 3)

$$\phi_{\mathrm{out}} = (\phi_{\mathrm{in}} + \Delta\phi_0)\mathrm{e}^{-\mathrm{j}\omega \frac{n_o}{c} L} = \phi_{\mathrm{in}} \mathrm{e}^{-\mathrm{j}\omega \frac{n_o}{c} L} + \Delta\phi.$$

Notice that PM block globally results as a linear, frequency-dispersive component.

B. AM Block Model

The interference block converts phase into amplitude modulation, thus simulating the operation of the output optical combiner. As well known, the AM transfer curve results as

$$\frac{P_{\mathrm{out}}}{P_{\mathrm{in}}} = \eta \left\{1 - 2\xi(1-\xi)\left[1 - \cos(\Delta\phi_U - \Delta\phi_L)\right]\right\}$$

where $\Delta\phi_U$ and $\Delta\phi_L$ are the electrooptic phase modulation induced, respectively, by the upper and lower modulator arm, and η is the device overall power efficiency. Here ξ denotes the optical beamsplitter asymmetry, which is specified as the power splitting ratio of the upper arm P_U/P_T, with P_U being the optical power flowing in the upper arm and $P_T = \eta P_{\mathrm{in}}$ the transmitted power.

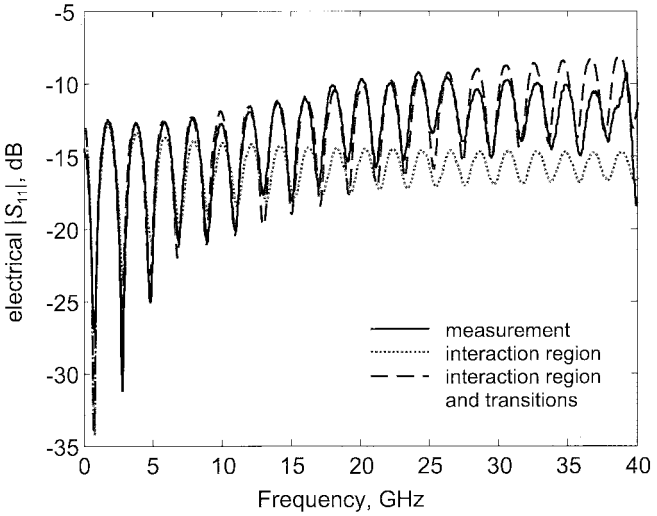

Fig. 4. Measured (solid) and modeled (dotted, dashed) electric return loss of the Corning-OTI modulator described in [12].

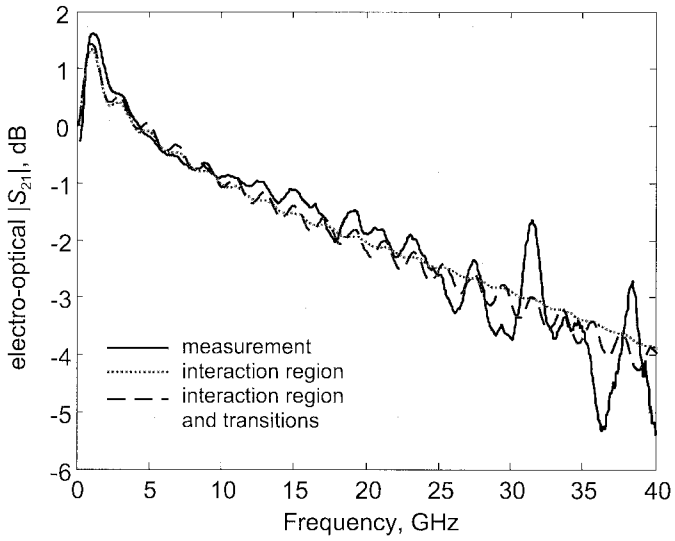

Fig. 5. Measured (solid) and modeled (dotted, dashed) normalized electrooptical response of the Corning-OTI modulator described in [12]. The electrooptical response is normalized to the low-frequency (100 MHz) value.

The instantaneous frequency chirping $\Delta f(t)$ can be expressed as

$$\Delta f(t) = \frac{1}{2\pi}\frac{\mathrm{d}\theta(t)}{\mathrm{d}t} = \frac{\mathrm{d}}{\mathrm{d}t}\arctan\left[\frac{\xi\sin\Delta\phi_U + (1-\xi)\sin\Delta\phi_L}{\xi\cos\Delta\phi_U + (1-\xi)\cos\Delta\phi_L}\right] \tag{4}$$

where $\theta(t)$ is the parasitic phase modulation of the AM signal. The interference block therefore results as a *nonlinear, memoryless* component; the time derivative in (4) can be readily carried out through an internal component in the circuit simulator.

Symmetric Mach–Zehnder modulators are common enough to suggest the implementation of a simplified model having only one PM block and an ad-hoc symmetrical interference block

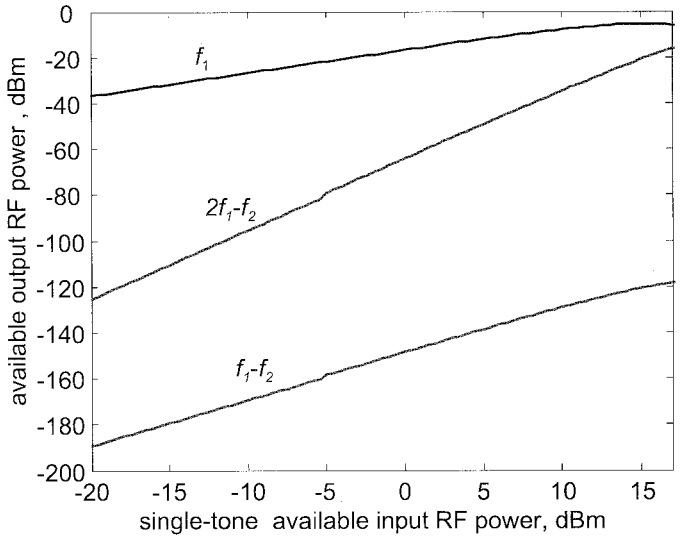

Fig. 6. Fundamental saturation and IMP generation under two-tone RF input signal. $f_1 = 5.18$ GHz, $f_2 = 5.19$ GHz.

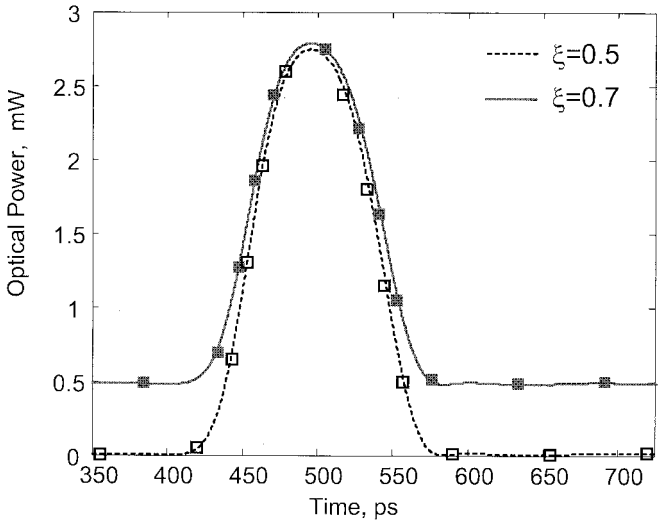

Fig. 7. Simulated amplitude response for single- and dual-arm modulator presented in [10]. Continuous curves: present model, squares: results from [10, Fig. 1].

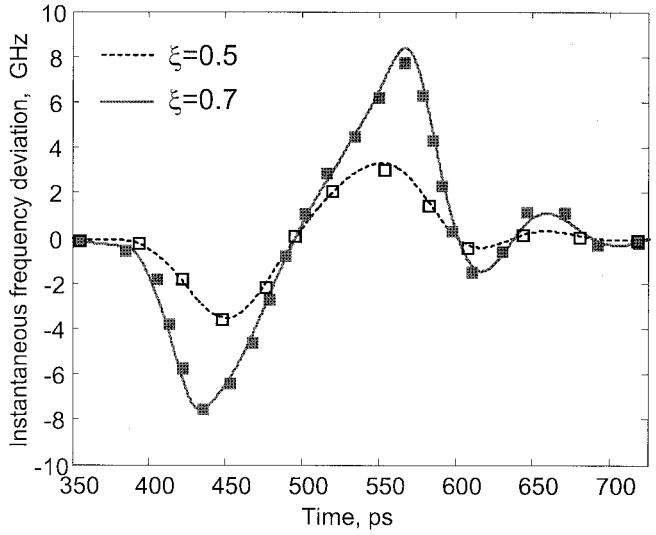

Fig. 8. Simulated instantaneous frequency deviation for the dual-arm modulator presented in [10]. Continuous curves: present model, squares: results from [10, Fig. 3].

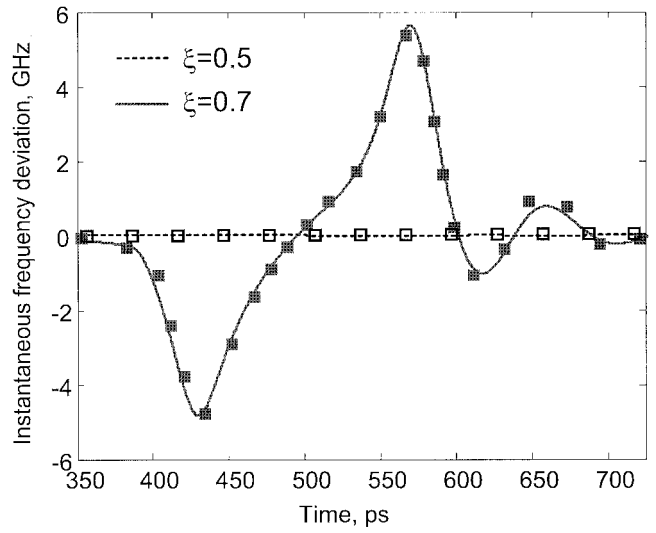

Fig. 9. Simulated instantaneous frequency deviation for the single-arm modulator presented in [10]. Continuous curves: present model, squares: results from [10, Fig. 2].

wherein $\Delta\phi_U = -\Delta\phi_L$. In this case, nonzero chirp can be obtained only if $\xi \neq 0.5$, i.e., the optical beamsplitter is asymmetrical [10].

III. Implementation

The PM and interference blocks have been implemented within MWOFFICE as a user-defined components by means of the MWOFFICE Model Wizard tool. The model source code is written in C++ language and can be compiled into a proper dynamic linked library. Once loaded as user-defined models, the PM and AM blocks can be directly connected to all the other available RF components. The PM block incorporates an accurate closed-form quasi-TEM analytical model for the coplanar line on an oxide-coated $LiNbO_3$ substrate [2]. This allows optimization to be performed directly on the geometrical line dimension. In the current version, the overlap integral between the optical and microwave fields is considered as an input parameter. Alternatively, when dealing with more complex or unconventional waveguiding structures, the frequency-dependent microwave electrode propagation characteristics, computed through more accurate external EM models [11], can be imported in the PM block as a lookup table file of frequency samples. In this case the electrooptical overlap integral can be directly evaluated from the RF line geometry and the optical field distribution. However, this approach is confined to the modulator analysis and cannot be applied to geometry optimization.

The splitting of the modulator model in two parts—one linear but frequency dispersive, the other nonlinear but memoryless—allows the simulations to be easily performed within the MWOFFICE environment, both in small-signal conditions, around a user specified bias, and in nonlinear (large-signal)

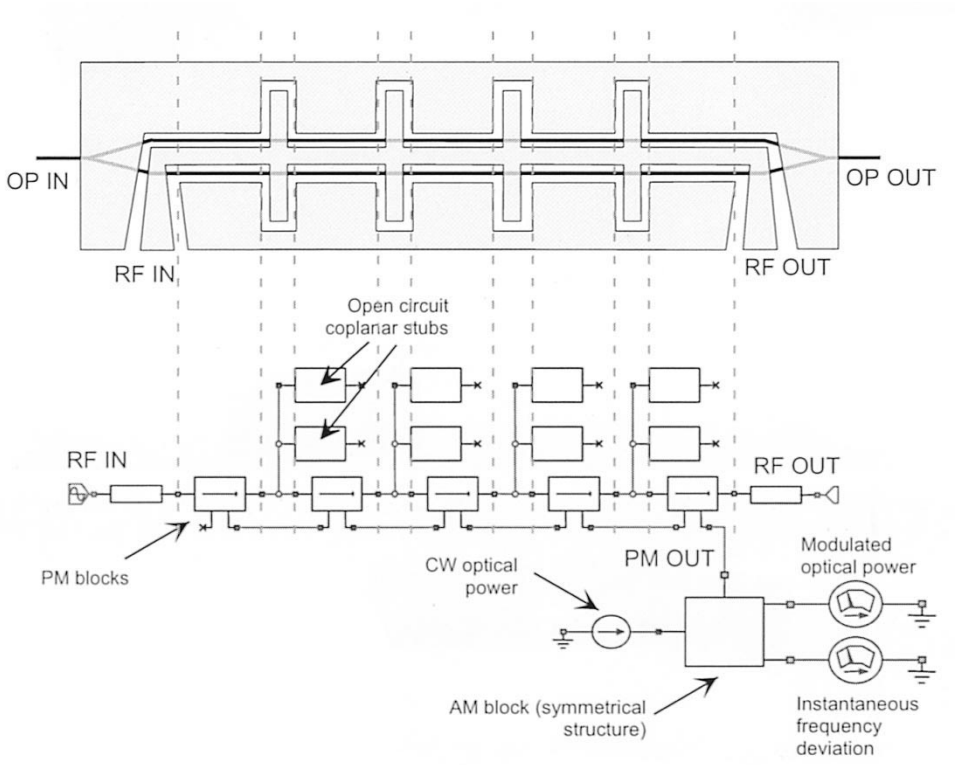

Fig. 10. Periodically loaded modulator [4] and its schematic representation. OP in the schematic refers to the optical power; notice the schematic for the open circuit stubs. Coplanar cross-sections are not introduced in the schematic shown.

quasi-periodic regime, thus allowing distortion and intermodulation performances to be directly simulated together with system-oriented features like eye diagrams. Implementation in other CAD environments (like the Agilent ADS) would also allow for general time-domain analysis of the modulator.

Finally, since the nonlinear AM block is separated from the phase-modulation section, the optimization of the modulator small-signal frequency response can be carried out, at least in the symmetric case, on the phase modulation response only, which (as already recalled) coincides with the AM small-signal response [8]. This procedure is computationally efficient since the PM block is linear, and therefore its optimization only requires the repeated use of the linear circuit solver. Large-signal analysis, being performed through computationally efficient techniques (such as the harmonic balance method), typically requires a few minutes CPU only on a Pentium processor; the CPU time of course also depends on the complexity of the circuit, on the number of harmonics, and on the excitation amplitude.

IV. Results

The modeling approach presented allows a wide class of electrooptic modulators to be analyzed and designed within a single CAD environment, regardless of structure complexity, thus avoiding the development of ad hoc models and enabling parasitic elements or other layout features to be incorporated at no additional cost.

As a first example, the model has been applied to study the performance of a broadband traveling-wave modulator fabricated by Corning-OTI. The device is a Mach–Zehnder interferometric modulator on a z-cut $LiNbO_3$ wafer, employing a thick coplanar waveguide (CPW) electrode terminated on a 30-Ω resistive load [12]. The small-signal electrical and optical performances of the modulator were characterized through on-wafer electrical and electrooptic measurements up to 40 GHz. The comparisons between the experimental and theoretical results in terms of electrical return loss and electrooptical response are reported in Figs. 4 and 5, respectively, showing a good agreement between modeled and measured data. The effect on the modulator performance of the tapered transitions is also highlighted. The propagation characteristics of the microwave electrode were simulated through a full-wave finite-element method approach [11]. Finally, in order to analyze the linearity of the modulator, we performed a two-tone simulation at input frequencies $f_1 = 5.18$ and $f_2 = 5.19$ GHz. The modulator was biased at quadrature $(V_\pi/2)$, and the incident optical power was 10 dBm. Fig. 6 shows the calculated second- and third-order intermodulation products (IMPs) and fundamental signal at the receiver. The generator and receiver impedances were set to 50 Ω, while the receiver responsivity is taken unitary.

To validate the capability of the approach of simulating the frequency chirping, two different device configurations have been studied, in case of both symmetrical $(\xi = 0.5)$ and asymmetrical optical splitting $(\xi = 0.7)$ (see [10]). The first sample is a dual arm modulator driven by a push–pull excitation ranging from zero to $V_\pi/2$ with the two arms respectively biased at zero and V_π V. The second kind of modulator is in single-arm configuration, i.e., the RF modulating signal is only applied to one arm; the two electrode biases are the same as that of the previous example, while the RF modulating signal is doubled. These samples have been chosen to compare the results obtained

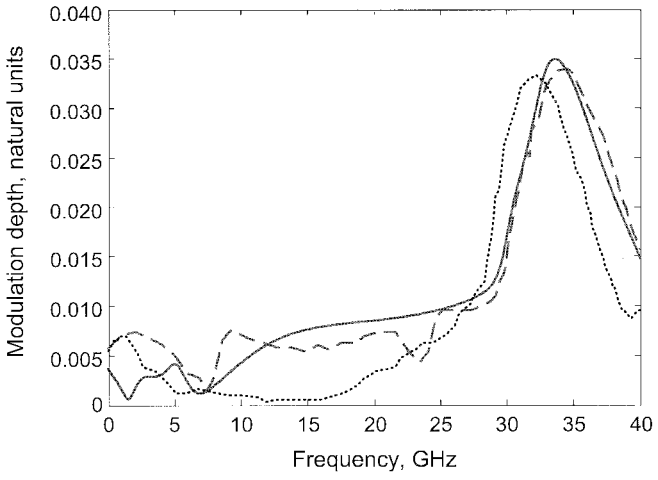

Fig. 11. Response of the six-section periodically loaded modulator reported in [4]. Continuous line: this work; dotted curve: Schaffner simulated response; dashed curve: measurements.

with that reported in [10]; the voltage modulating pulse is modeled as in [10] and [13]. Fig. 7 shows the modulator output for the two cases, while Figs. 8 and 9 report the simulation results concerning the dual- and the single-arm modulator, respectively, for $\xi = 0.5$, $\xi = 0.7$ (corresponding to $P_2/P_T = 0.5$ and $P_2/P_T = 0.3$ in [10]). Notice the presence of nonzero chirp even in the case of $\xi = 0.5$ for the single-arm configuration modulator due to the unbalanced RF excitation applied to the interferometer arms. The results obtained are in excellent agreement with those reported in [10].

Finally, we consider the periodically loaded modulator in [4], shown in Fig. 10 with the circuit schematic; for the sake of simplicity, the schematic shown is of a modulator with only four sections. Since the structure is symmetrical, only one arm is modeled and a symmetric AM block is introduced. The frequency response of a six-section device simulated with the present model is compared in Fig. 11 with the experimental and simulated data from [4], with good agreement. The modulator was simulated using the geometrical parameters in [4] and exploiting the CPW model in [2].

V. Conclusion

A full small- and large-signal model for electrooptic amplitude modulators embedded within a CAD environment for circuit analysis and optimization has been presented, together with a few examples of application. In its current implementation, the model yields both the output power modulation and the frequency chirping of the optical output signal. The model provides a CAD tool for the design and optimization of several classes of wide- and narrow-bandwidth modulators, and allows parasitic effects such as transitions, launchers, and nonideal loads to be directly incorporated into the RF model.

Acknowledgment

The assistance of Corning-OTI and the AWR technical staff is kindly acknowledged.

References

[1] Microwave Office 2000 RF Design Suite ver. 3.22, Applied Wave Research Inc..

[2] G. Ghione, M. Goano, G. Madonna, G. Omegna, M. Pirola, S. Bosso, D. Frassati, and A. Perasso, "Microwave modeling and characterization of thick coplanar waveguides on oxide-coated lithium niobate substrates for electro-optical applications," *IEEE Trans. Microwave Theory Tech.*, vol. 47, pp. 2287–2293, Dec. 1999.

[3] K. W. Hui, K. S. Chiang, B. Y. Wu, and Z. H. Zhang, "Electrode optimization for high-speed traveling-wave integrated optic modulator," *J. Lightwave Technol.*, vol. 16, pp. 232–238, Feb. 1998.

[4] J. H. Schaffner and R. R. Hayes, "Velocity-matching in millimeter wave integrated optic modulators with periodic electrodes," *J. Lightwave Technol.*, vol. 12, pp. 503–511, Mar. 1994.

[5] R. Krähenbühl and M. M. Howerton, "Investigations on short-path-length high-speed optical modulators in $\mathrm{LiNbO_3}$ with resonant-type electrodes," *J. Lightwave Technol.*, vol. 19, pp. 1287–1297, Sept. 2001.

[6] G. K. Gopalakrishnan, W. K. Burns, R. W. McElhanon, C. H. Bulmer, and A. S. Greenblatt, "Performance and modeling of broadband $\mathrm{LiNbO_3}$ traveling wave optical intensity modulators," *J. Lightwave Technol.*, vol. 12, no. 10, pp. 1807–1819, Oct. 1994.

[7] R. Krähenbühl and W. K. Burns, "Modeling of broad-band traveling-wave optical-intensity modulators," *IEEE Trans. Microwave Theory Tech.*, vol. 48, pp. 860–864, May 2000.

[8] R. C. Alferness, "Waveguide electrooptic modulators," *IEEE Trans. Microwave Theory Tech.*, vol. MTT-30, pp. 1121–1137, Aug. 1982.

[9] G. P. Agrawal and N. K. Dutta, *Semiconductor Lasers*, 2nd ed. New York: Van Nostrand Reinhold, 1993.

[10] J. C. Cartledge, "Performance of 10 Gbps lightwave systems based on lithium niobate Mach-Zehnder modulators with asymmetric Y-branch waveguides," *IEEE Photon. Technol. Lett.*, vol. 7, pp. 1090–1092, Dec. 1995.

[11] F. Bertazzi, O. A. Peverini, M. Goano, G. Ghione, R. Orta, and R. Tascone, "A fast reduced-order model for the full-wave FEM analysis of lossy inhomogeneous anisotropic waveguides," *IEEE Trans. Microwave Theory Tech.*, vol. 50, pp. 2108–2114, Sept. 2002.

[12] G. Giarola, "Progetto, realizzazione e misura di un modulatore a larga banda in Ti: $\mathrm{LiNbO_3}$ Z-cut," Master thesis, Politecnico di Torino, Italy, Oct. 2001.

[13] J. C. Cartledge, C. Rolland, S. Lemerle, and A. Solheim, "Theoretical performance of 10 Gb/s lightwave systems using a III-V semiconductor Mach-Zehnder modulator," *IEEE Photon. Technol. Lett.*, vol. 6, pp. 282–284, Feb. 1994.

Marco Pirola (M'96) was born in Velezzo Lomellina, Italy, in 1963. He received the Laurea degree in electronic engineering and the Ph.D. degree from Politecnico di Torino, Italy, in 1987 and 1992, respectively.

In 1992 and 1994, he was a Visiting Researcher at the Hewlett Packard Microwave Technology Division, Santa Rosa, CA. Since 1992, he has been a Researcher in the Electronic Department of Politecnico di Torino, where his research concerns the simulation, modeling, and measurements of microwave devices and systems.

Federica Cappelluti (S'02–M'03) was born in Ortona, Italy, in 1973. She received the Laurea degree in electronic engineering and the Ph.D. degree in electronic and communications engineering from the Politecnico di Torino, Italy, in 1998 and 2002, respectively.

She is currently a Research Assistant in the Dipartimento di Elettronica, Politecnico di Torino. Her research interests concern the modeling and simulation of modulators and photodiodes for RF-on-fiber and high-speed optical communications systems. She is also involved in research on power microwave devices and circuits, with emphasis on electrothermal modeling and stability issues.

Giovanni Giarola, photograph and biography not available at the time of publication.

Giovanni Ghione (M'87–SM'94) was born in Alessandria, Italy, in 1956. He graduated in electronic engineering (cum laude) from Politecnico di Torino, Italy, in 1981.

In 1983, he joined Politecnico di Torino as a Research Assistant. From 1987 to 1990, he was an Associate Professor with Politecnico di Milano. In 1990, he joined the University of Catania as a full Professor of electronics. Since 1991, he has held the same position with the Faculty of Engineering, Politecnico di Torino. Since 1981, he has been engaged in Italian and European research projects (ESPRIT 255, COSMIC, and MANPOWER) in the field of active and passive microwave CAD. His present research interests concern the physics-based simulation of active microwave and optoelectronic devices, with particular attention to noise modeling, thermal modeling, and active device optimization. His research interests also include several topics in computational electromagnetics, including coplanar component analysis. He has published more than 150 papers and book chapters in the above fields.

Prof. Ghione is a member of the Associazione Elettrotecnica Italiana. He is a member of the Editorial Board of the IEEE TRANSACTIONS ON MICROWAVE THEORY AND TECHNIQUES.